Available on CMS information server

CMS NOTE 2004/017

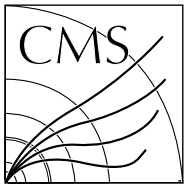

The Compact Muon Solenoid Experiment

CMS Note

Mailing address: CMS CERN, CH-1211 GENEVA 23, Switzerland

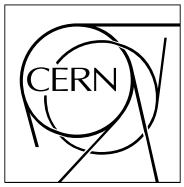

20 August 2004

Heavy Charged MSSM Higgs Bosons in the $\mathrm{H}^{\pm} \rightarrow \mathrm{tb}$ Decay in CMS

S. Lowette[a)] and J. Heyninck

Vrije Universiteit Brussel (VUB) – IIHE, Brussels, Belgium

P. Vanlaer

Université Libre de Bruxelles (ULB) – IIHE, Brussels, Belgium

Abstract

In this note the prospects to discover a heavy charged MSSM Higgs boson in the $\mathrm{H}^{\pm} \rightarrow \mathrm{tb}$ decay channel are presented, with the tagging of three b quarks. The main background from $\mathrm{t\bar{t}} + \mathrm{jets}$, with real additional b jets or a jet mistagged as b, is kinematically very similar to the signal. The study is performed with fast detector simulation. This analysis includes a dedicated background simulation, a study of HLT trigger acceptance, advanced b tagging and reconstruction results, and an estimation of the influence of the systematic uncertainties on the background cross section. Furthermore, improvements are considered from the possible knowledge of the charged Higgs boson mass and from exploiting the fully hadronic decay channel. The discovery reach is investigated, and it is concluded that, with the present analysis, no visibility is left in the MSSM parameter space for this channel.

[a)] email: steven.lowette@cern.ch

1 Introduction

One of the most straightforward ways to extend the Higgs sector of the Standard Model is to add an extra complex Higgs doublet to the theory, thus giving rise to a general two Higgs doublet model (2HDM). In such a model five physical Higgs bosons arise after electroweak symmetry breaking [1]. Three of them are neutral (the scalars h and H and the pseudoscalar A), the other two are charged (the scalars $\mathrm{H}^{\pm}$). A particular example of a model containing such a 2HDM extension of the Higgs sector is the Minimal Supersymmetric Standard Model (MSSM).

To describe the production cross section and decay modes of the charged Higgs boson $\mathrm{H}^{\pm}$ in terms of the free parameters of the MSSM, only to of these parameters are needed at tree level. These parameters are usually taken as the ratio of the vacuum expectation values of the two Higgs doublets $\tan\beta = v_2/v_1$ and the mass of the pseudoscalar Higgs boson m_{A}. The charged Higgs boson mass is related to m_{A}, at tree level, by the relation

$$m_{\mathrm{H}^{\pm}} = \sqrt{m_{\mathrm{A}}^2 + m_{\mathrm{W}^{\pm}}^2}. \tag{1}$$

The branching fractions for the decay channels of the charged Higgs boson depend strongly on its mass. As shown in Fig. 1, for masses below $m_{\mathrm{t}} + m_{\mathrm{b}}$, the $\mathrm{H}^{\pm} \to \tau\nu$ channel dominates ($\tan\beta > 1$). For larger masses, the channel

$$\mathrm{H}^{\pm} \to \mathrm{tb} \tag{2}$$

opens up. The latter, in the dominant production channel $\mathrm{gb} \to \mathrm{tH}^{\pm}$, results in complex final states. The most interesting one is the semileptonic final state

$$\mathrm{gb} \to \mathrm{tH}^{\pm} \to \mathrm{ttb} \to \mathrm{W}^{+}\mathrm{W}^{-}\mathrm{bbb} \to \mathrm{qq}'\ell\nu\mathrm{bbb}, \tag{3}$$

because the Higgs boson mass can still be reconstructed, and an isolated lepton is present to trigger on.

The potential of the decay channel (2) for large Higgs boson masses at the LHC has been considered before at parton level in several phenomenological studies [2–6]. These studies showed the possibility of detecting the charged Higgs boson in certain regions of the $(m_{\mathrm{A}}, \tan\beta)$ parameter space during the low luminosity run of the LHC, with both three or four b jets tagged, provided good b–tagging capabilities to suppress the very large, and kinematically very similar $\mathrm{t\bar{t}} + \mathrm{jets}$ background. Fast simulation studies, which take into account parametrized detector performance, have also been carried out for CMS [7] and ATLAS [8, 9].

In this analysis, charged Higgs boson detection was studied for the final state (3) using triple b tagging, during the low luminosity period, where the LHC will operate at $\mathcal{L} = 2 \times 10^{33}\,\mathrm{cm}^{-2}\mathrm{s}^{-1}$ and acquire an integrated luminosity of $L = \int \mathcal{L}\,dt = 60\,\mathrm{fb}^{-1}$. Production of the $\mathrm{H}^{\pm}$ bosons through heavy sparticle cascades is not taken into account in this study. Additionally, supersymmetric particles are supposed to be heavy enough, so that supersymmetric decays of the $\mathrm{H}^{\pm}$ can be neglected. It has indeed been argued before [7] that for a heavy SUSY spectrum, the branching fraction for (2) is only slightly affected by SUSY decay channels opening up, for not too large Higgs boson masses ($m_{\mathrm{H}^{\pm}} < 500\,\mathrm{GeV}/c^2$).

The main improvement of this analysis with respect to the earlier studies is the inclusion of the most recent results [10] on the theoretical calculation for the signal cross section at leading order (LO) and next–to–leading order (NLO), resulting in sizeable effects compared to the previous discovery prospects. Indeed, the leading order cross section values, predicted by the Monte–Carlo program `PYTHIA` [11] have decreased by a factor ~ 3 over the last 5 years[1)], as shown in Fig. 2. Other improvements are the use of a new dedicated background simulation, the inclusion of the acceptance of the CMS triggers, the introduction of a likelihood based method to suppress the combinatorial background, the estimate of systematic uncertainties on the background cross section and the estimate of the usability of fully hadronic decays.

To start with, in Section 2 signal and background simulations are described in detail. Next, in Section 3, event selection and triggering are discussed. In Section 4 the likelihood method to choose the best solution is outlined. Then the results of this analysis are presented in Sections 5.1 and 5.2, and systematic uncertainties on the background are discussed in Section 5.3. Finally the use of the fully hadronic decay channel is discussed in Section 6.

[1)] As an example, a decrease was noticed because of a different running b–mass value from version `6.205` on. Since a bug fix in version `6.218` during the 2003 Les Houches Workshop on Physics at TeV Colliders, the `PYTHIA` output now corresponds to the theoretical calculation.

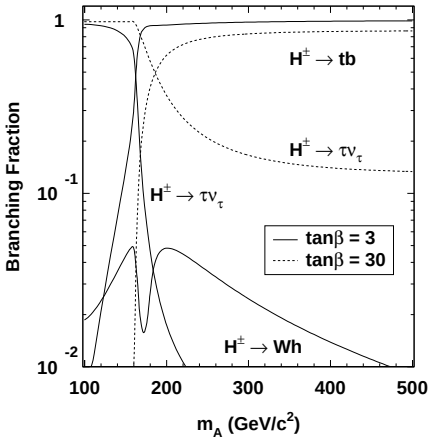

Figure 1: Charged Higgs boson branching fractions as a function of m_{A}, generated with HDECAY.

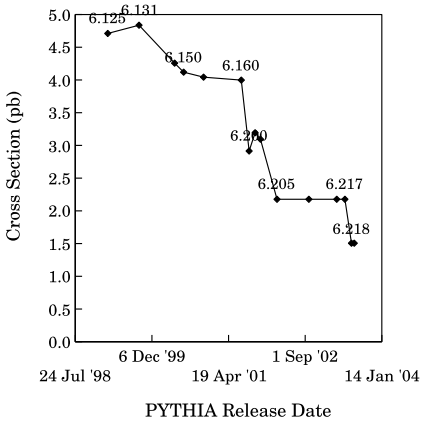

Figure 2: Evolution with time of the PYTHIA predicted cross section value for $\mathrm{gb} \to \mathrm{tH}^{\pm}$. The PYTHIA version is shown in the labels on the curve. ($m_{\mathrm{A}} = 300\,\mathrm{GeV}/c^2$, $\tan\beta = 50$)

2 Signal and Background

2.1 Signal simulation

The production of the charged Higgs boson is considered in the dominant inclusive channel $\mathrm{pp} \to \mathrm{tH}^{\pm}\mathrm{X}$ with an associated top quark. The exclusive process $\mathrm{gg} \to \mathrm{tbH}^{\pm}$ should not be used to calculate the LO cross section when only three b–tagged jets are required. Indeed, the computation of this process at tree level is only reliable when a minimum transverse momentum on the spectator b quark is imposed. Such a result is however not correct when the spectator b may escape at large rapidity. Therefore the bottom parton approximation, where the potential large logarithms in the perturbation series are resummed, should be used. At leading order, the cross section for the process $\mathrm{pp} \to \mathrm{tH}^{\pm}\mathrm{X}$ should then be evaluated in the channel $\mathrm{gb} \to \mathrm{tH}^{\pm}$ [10].

The signal cross section is sensitive to the two parameters $\tan\beta$ and m_{A}. As the $\bar{\mathrm{t}}\mathrm{bH}^{+}$ Yukawa Lagrangian term can be written as

$$\frac{gV_{\mathrm{tb}}}{\sqrt{2}\,m_{\mathrm{W}^{\pm}}}\mathrm{H}^{+}(m_{\mathrm{t}}\cot\beta\,\bar{\mathrm{t}}\,\mathrm{b}_L + m_{\mathrm{b}}\tan\beta\,\bar{\mathrm{t}}\,\mathrm{b}_R), \tag{4}$$

the cross section is enhanced at small and large values of $\tan\beta$, with a minimum at $\tan\beta = \sqrt{m_{\mathrm{t}}/m_{\mathrm{b}}} \approx 6$. Furthermore, the cross section decreases rapidly with rising m_{A}. Typically, it decreases an order of magnitude as m_{A} increases from $250\,\mathrm{GeV}/c^2$ to $500\,\mathrm{GeV}/c^2$, and when going from $\tan\beta = 30$ down to the minimum. These cross section dependencies on $\tan\beta$ and m_{A} are shown in Figs. 3 and 4. For a few values of $\tan\beta$ and m_{A}, the $\mathrm{gb} \to \mathrm{tH}^{\pm}$ cross section at the LHC are also summarized in Table 1.

Table 1: Leading–order cross section values for $\mathrm{pp} \to \mathrm{tH}^{\pm}\mathrm{X}$ for several values of the $\tan\beta$ and m_{A} parameters.

m_{A}	$\tan\beta = 3$	$\tan\beta = 10$	$\tan\beta = 30$	$\tan\beta = 50$
$300\,\mathrm{GeV}/c^2$	214 fb	78 fb	531 fb	1473 fb
$400\,\mathrm{GeV}/c^2$	92 fb	33 fb	227 fb	630 fb
$500\,\mathrm{GeV}/c^2$	42 fb	15 fb	104 fb	289 fb

The calculation of the signal has also been performed at NLO [10]. The resulting increase in the cross section depends on the value of the MSSM parameters. In the region $\tan\beta > 30$ limiting this analysis the k factor is constant ($k = 1.3$) for $250 < m_{\mathrm{A}} < 500\,\mathrm{GeV}/c^2$. In Table 2, the cross section at NLO is given for some typical values of $\tan\beta$ and m_{A}.

The generation of the signal was performed with PYTHIA 6.125, with the requirement that the charged Higgs boson decays to t and b quarks. The branching fraction $\mathrm{BR}(\mathrm{H}^{\pm} \to \mathrm{tb})$ for this decay process, calculated with HDECAY 3.0 [12], ranges between $\sim 80\%$ for small m_{A} and large $\tan\beta$ and $\sim 100\%$ for large m_{A} and small

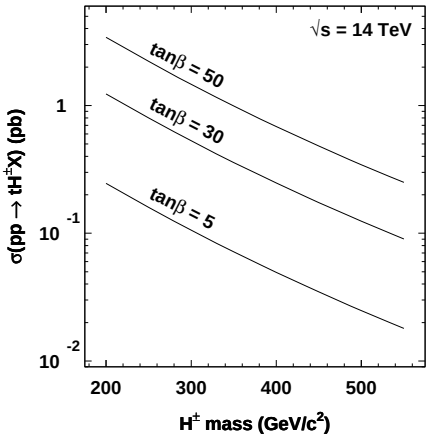

Figure 3: Cross section for $\mathrm{pp} \to \mathrm{tH^{\pm}X}$ as a function of m_{A}.

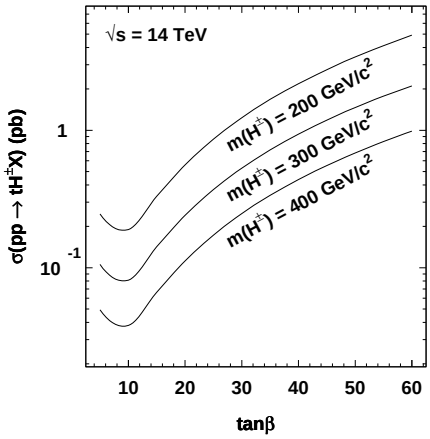

Figure 4: Cross section for $\mathrm{pp} \to \mathrm{tH^{\pm}X}$ as a function of $\tan\beta$.

Table 2: Next–to–leading order cross section values for $\mathrm{pp} \to \mathrm{tH^{\pm}X}$ for several values of the $\tan\beta$ and m_{A} parameters.

m_{A}	$\tan\beta = 10$	$\tan\beta = 30$	$\tan\beta = 50$
$300\,\mathrm{GeV}/c^2$	111 fb	686 fb	1896 fb
$400\,\mathrm{GeV}/c^2$	47 fb	293 fb	815 fb
$500\,\mathrm{GeV}/c^2$	21 fb	134 fb	384 fb

$\tan\beta$, as also shown in Fig. 1. Finally, the total number of events for a given set of parameters can be obtained as

$$N = \sigma(\mathrm{pp} \to \mathrm{tH^{\pm}X}) \times \mathrm{BR}(\mathrm{H^{\pm}} \to \mathrm{tb}) \times L, \tag{5}$$

where L is the integrated luminosity, and σ is obtained from [10, 13].

Six samples were generated at $\tan\beta = 50$ and masses m_{A} ranging from 250 to $500\,\mathrm{GeV}/c^2$. All possible decays of the two top quarks are considered. The number of signal events from (5) before the event selection is almost 55 000 for $m_{\mathrm{A}} = 250\,\mathrm{GeV}/c^2$ down to about 7 500 for $m_{\mathrm{A}} = 500\,\mathrm{GeV}/c^2$, for an integrated luminosity of $30\,\mathrm{fb}^{-1}$.

2.2 Background simulation

At leading order, the dominant background comes from Standard Model $\mathrm{gb} \to \mathrm{t\bar{t}b}$ and $\mathrm{t\bar{t}} + \mathrm{jet}$ production, where in the latter the accompanying quark or gluon jet is misidentified as a b jet. Other potential multi–jet backgrounds are much smaller [2, 14] and neglected here.

The aforementioned background processes are not explicitly implemented in PYTHIA. Therefore the simulation of the background has in the first place been performed by generating $\mathrm{t\bar{t}}$ events with PYTHIA 6.125, with the processes 81 and 82 for heavy quark pair production, where the PYTHIA parton shower generates additional jets. An overall LO cross section of $560\,\mathrm{pb}$ was used, resulting in about 1.7×10^7 events before the event selection, for $30\,\mathrm{fb}^{-1}$ of integrated luminosity. For the decay of these background events, no constraints are applied, such that all the available channels for the $\mathrm{W^{\pm}}$ decays are considered. This background is further referred to in this paper as the $\mathrm{t\bar{t}}$ background.

It should be remarked that for a consistent description of the backgrounds at leading order, the event simulation has to be performed starting from the hard interactions $\mathrm{pp} \to \mathrm{t\bar{t}b}$ and $\mathrm{pp} \to \mathrm{t\bar{t}j}$. For this purpose, the matrix element generator MadGraph/MadEvent [15] was used. The events were generated with a cut on the transverse momentum ($p_T > 10\,\mathrm{GeV}/c$) and the pseudorapidity ($|\eta| < 2.5$) of the extra jet accompanying the tops, in order to keep the cross section finite. This generation resulted in a total cross section of $678\,\mathrm{pb}$, or over 2.0×10^7 events before selection. After the simulation of the hard interaction, the events were interfaced to PYTHIA for parton showering, decay and hadronization, using the same parameters as for the $\mathrm{t\bar{t}}$ generation. In the following, this background is called the $\mathrm{t\bar{t}b}/\mathrm{t\bar{t}j}$ background.

The calculation for $\mathrm{t\bar{t}}$ at NLO is available, and the cross section scales up to about $800\,\mathrm{pb}$, depending on, for example, the scale choice and the top mass [16]. This rise was taken into account by using a k factor of 1.43 for the $\mathrm{t\bar{t}}$ background. It leads to 2.4×10^7 events to be considered before selection and triggering. The NLO calculation for the processes $\mathrm{pp} \to \mathrm{t\bar{t}b}$ and $\mathrm{pp} \to \mathrm{t\bar{t}j}$ has not been performed yet. Therefore, no NLO comparison was made for this background.

3 Event Selection and Triggering

3.1 b–tagging simulation

To simulate the detector performance, the fast simulation program `CMSJET 4.801` [17] was used. This program uses track smearing with the fast tracker simulation `FATSIM` as a basis for b tagging. In this study b tagging is performed by requiring two charged particle tracks with $p_T > 0.9\,\mathrm{GeV}/c$ in a circle of radius $R = 0.4\,\mathrm{rad}$ in the (η, ϕ) plane around the jet direction. The impact parameter (IP) of these tracks is further constrained by the cut $\mathrm{IP} < 2\,\mathrm{mm}$. Finally a cut $S_{\mathrm{IP}} > x$ is applied on their IP significance $S_{\mathrm{IP}} = \mathrm{IP}/\Delta_{\mathrm{IP}}$, defined as the ratio of the IP of the track and its uncertainty Δ_{IP}. The b–tagging parameter x can now be used to raise or reduce the b–tagging efficiency, respectively to reduce or raise the purity.

The b–jet tagging efficiency and the purities when tagging light and charm jets were estimated on all background and signal samples, by comparing reconstructed objects to particles at generator level. For $x > 2.5$, the efficiency and purities are summarized in Table 3. The values obtained show an increasing b–tagging efficiency for harder event kinematics, along with increasing c–quark and light jet mistag rates. Another observation is the increased efficiency and especially mistag rate in the $\mathrm{t\bar{t}b}/\mathrm{t\bar{t}j}$ background compared to the $\mathrm{t\bar{t}}$ background. From this observation it can be deduced, that the spectrum of the b jets in the $\mathrm{t\bar{t}}$ background is softer than in the $\mathrm{t\bar{t}b}/\mathrm{t\bar{t}j}$ background.

Table 3: b–tagging efficiency and purities for background and signal, with $x > 2.5$.

	b–tagging efficiency	total mistag rate	c–quark mistag rate	light jet mistag rate
$\mathrm{t\bar{t}}$ background	44.7%	2.38%	9.5%	0.92%
$\mathrm{t\bar{t}b}/\mathrm{t\bar{t}j}$ background	45.9%	2.54%	9.9%	1.02%
$\mathrm{tH^{\pm}}$ ($m_{\mathrm{A}} = 250\,\mathrm{GeV}/c^2$)	43.9%	2.57%	9.8%	1.10%
$\mathrm{tH^{\pm}}$ ($m_{\mathrm{A}} = 300\,\mathrm{GeV}/c^2$)	46.4%	2.61%	10.0%	1.13%
$\mathrm{tH^{\pm}}$ ($m_{\mathrm{A}} = 350\,\mathrm{GeV}/c^2$)	48.1%	2.66%	10.2%	1.16%
$\mathrm{tH^{\pm}}$ ($m_{\mathrm{A}} = 400\,\mathrm{GeV}/c^2$)	49.2%	2.71%	10.2%	1.23%
$\mathrm{tH^{\pm}}$ ($m_{\mathrm{A}} = 450\,\mathrm{GeV}/c^2$)	50.0%	2.75%	10.5%	1.25%
$\mathrm{tH^{\pm}}$ ($m_{\mathrm{A}} = 500\,\mathrm{GeV}/c^2$)	50.7%	2.89%	11.0%	1.32%

These results are not directly comparable to the full simulation studies on the CMS b–tagging capabilities that were performed on inclusive jet samples [18]; they are, however, found to be in reasonable agreement.

To obtain measurements for b–tagging efficiency and purity from data, other methods have to be used. For CDF at the Tevatron, measurements on data are for example performed on $\mathrm{b\bar{b}}$ pairs as described in [19]. At the LHC, the semileptonic decay of a $\mathrm{t\bar{t}}$ pair seems an interesting channel to evaluate the efficiency, as highly b–enriched data samples could be obtained. With a selection as in [14], a 1% statistical uncertainty on the b–tagging efficiency can be reached with $20\,\mathrm{fb}^{-1}$ of integrated luminosity.

3.2 Minimal selection criteria

In order to reconstruct an event, some minimal requirements must be met. As the final state of the $\mathrm{tH^{\pm}}$ decay consists of at least three b jets, two other jets, an isolated lepton and missing energy, only those events are accepted for which `CMSJET` finds at least

- one isolated lepton (electron or muon) with $|\eta| < 2.4$ and $p_T > 19\,\mathrm{GeV}/c$ for muons and $p_T > 29\,\mathrm{GeV}/c$ for electrons. Isolation is ensured by requiring the energy in a cone $\Delta R = \sqrt{\Delta\phi^2 + \Delta\eta^2} = 0.3\,\mathrm{rad}$ around the lepton to be smaller than 10% of the lepton energy.

- five jets (b or non b) with $p_T > 20\,\mathrm{GeV}/c$ and $|\eta| < 2.4$. Jets are reconstructed with a so–called "modified UA1 jet finder" algorithm, using calorimeter information. It looks for jets in a cone of $\Delta R = 0.5\,\mathrm{rad}$ with a mobile centre, starting from the cells with highest E_T and muon hits. Detailed information can be found in the CMSJET manual [17] and references therein.
- three jets with $x > 2.5$, considered further on as b jets and two other jets with $x < 2.5$, considered as non–b jets.

The efficiencies of these three minimal selection criteria on the different background and signal samples are shown in Table 4 for $\tan\beta = 50$ and $30\,\mathrm{fb}^{-1}$ of integrated luminosity.

Table 4: Efficiencies of the minimal selection criteria to allow for an event reconstruction.

$\tan\beta = 50$, 30 fb^{-1}	# events before cuts	one isolated lepton	three b jets	five jets
$\mathrm{t\bar{t}}$ background	16 800 000	4 211 928 (25.1%)	32 456 (0.77%)	15 736 (48.5%)
$\mathrm{t\bar{t}b/t\bar{t}j}$ background	20 340 000	5 059 168 (24.9%)	46 249 (0.91%)	23 593 (51.0%)
$\mathrm{tH^{\pm}}$ ($m_\mathrm{A} = 250\,\mathrm{GeV}/c^2$)	54 644	12 782 (23.4%)	1 105 (8.64%)	769 (69.6%)
$\mathrm{tH^{\pm}}$ ($m_\mathrm{A} = 300\,\mathrm{GeV}/c^2$)	36 681	8 565 (23.4%)	933 (10.9%)	659 (70.6%)
$\mathrm{tH^{\pm}}$ ($m_\mathrm{A} = 350\,\mathrm{GeV}/c^2$)	23 988	5 667 (23.6%)	686 (12.1%)	492 (71.8%)
$\mathrm{tH^{\pm}}$ ($m_\mathrm{A} = 400\,\mathrm{GeV}/c^2$)	16 176	3 849 (23.8%)	522 (13.6%)	381 (72.9%)
$\mathrm{tH^{\pm}}$ ($m_\mathrm{A} = 450\,\mathrm{GeV}/c^2$)	10 888	2 618 (24.0%)	362 (13.8%)	270 (74.7%)
$\mathrm{tH^{\pm}}$ ($m_\mathrm{A} = 500\,\mathrm{GeV}/c^2$)	7 472	1 785 (23.9%)	263 (14.7%)	198 (75.2%)

The small efficiencies for the selection are mainly due to two reasons. First, only ∼45% of the decays are semileptonic, and so the other 55% of the decays are already expected to be suppressed when requiring the isolated lepton and the two extra jets.

For the lepton, the selection was further refined. In Table 5, the efficiency is shown separately for the isolation criterion only, for the transverse momentum cut $p_T > 19/29\,\mathrm{GeV}/c$ only, and for both cuts, for all signal and background samples for $\tan\beta = 50$ and $30\,\mathrm{fb}^{-1}$ of integrated luminosity. For the cut on p_T, an increasing efficiency is observed for larger values of m_A, corresponding to harder signal event kinematics. The behaviour of the lepton isolation requirement, which is the dominating effect for the lepton selection, is less obvious. Especially the discrepancy between background and signal is not clear, and requires a more detailed analysis to understand.

Table 5: Efficiencies to select an isolated lepton and/or a lepton above a defined p_T threshold.

$\tan\beta = 50$, $30\,\mathrm{fb}^{-1}$	# events before cuts	at least one isolated lepton	at least one lepton above p_T threshold	at least one lepton satisfying both cuts
$\mathrm{t\bar{t}}$ background	16 800 000	4 718 952 (28.1%)	6 141 408 (36.6%)	4 211 928 (25.1%)
$\mathrm{t\bar{t}b/t\bar{t}j}$ background	20 340 000	5 632 756 (27.7%)	7 672 451 (37.7%)	5 059 168 (24.9%)
$\mathrm{tH^{\pm}}$ ($m_\mathrm{A} = 250\,\mathrm{GeV}/c^2$)	54 644	14 194 (26.0%)	21 791 (39.9%)	12 782 (23.4%)
$\mathrm{tH^{\pm}}$ ($m_\mathrm{A} = 300\,\mathrm{GeV}/c^2$)	36 681	9 511 (25.9%)	15 413 (42.0%)	8 565 (23.4%)
$\mathrm{tH^{\pm}}$ ($m_\mathrm{A} = 350\,\mathrm{GeV}/c^2$)	23 988	6 264 (26.1%)	10 571 (44.1%)	5 667 (23.6%)
$\mathrm{tH^{\pm}}$ ($m_\mathrm{A} = 400\,\mathrm{GeV}/c^2$)	16 176	4 230 (26.2%)	7 462 (46.1%)	3 849 (23.8%)
$\mathrm{tH^{\pm}}$ ($m_\mathrm{A} = 450\,\mathrm{GeV}/c^2$)	10 888	2 860 (26.3%)	5 159 (47.4%)	2 618 (24.0%)
$\mathrm{tH^{\pm}}$ ($m_\mathrm{A} = 500\,\mathrm{GeV}/c^2$)	7 472	1 953 (26.1%)	3 639 (48.7%)	1 785 (23.9%)

The second and main part of the inefficiency comes from the requirement of three b–tagged jets, which allows the background to be suppressed by one order of magnitude more than the signal. When comparing this efficiency for the $\mathrm{t\bar{t}b/t\bar{t}j}$ background with the $\mathrm{t\bar{t}}$ background, an increase in efficiency is observed, due to the increased b–tagging efficiency and especially mistag rate, previously shown in Table 3.

Finally, the third requirement for five jets with $p_T > 20\,\mathrm{GeV}/c$ reveals once more the harder event kinematics as m_A increases. This cut also shows the difference in hardness between the two backgrounds.

3.3 High Level Trigger (HLT) selection

In order to estimate the influence of the CMS trigger acceptance on the reconstructable event rate, the High–Level Trigger (HLT) cuts are applied only after the minimal selection criteria presented in Section 3.2. As an isolated lepton is present in the final state, high triggering efficiencies are expected with only the inclusive electron and muon triggers. The HLT cuts at low luminosity are $29\,\mathrm{GeV}/c$ for single electrons and $19\,\mathrm{GeV}/c$ for single muons [18].

Full simulation studies on electrons from $\mathrm{W}^{\pm} \to \mathrm{e}\nu$ have shown that, for electrons in the fiducial volume of the calorimeter, with a generated $p_T > 29\,\mathrm{GeV}/c$, the combined Level–1 and HLT trigger efficiencies are expected to be 67.1% [18]. With CMSJET, however, the HLT single electron cut on such electrons for this signal and backgrounds was found to be 97% efficient. Therefore, an additional correction factor of 68.9% on the obtained CMSJET HLT selection efficiency was applied for electrons, to take into account this inefficiency.

The results of the event selection and triggering for the backgrounds and the different signal samples are summarized in Table 6, for $\tan\beta = 50$ and $30\,\mathrm{fb}^{-1}$ of integrated luminosity. About 85% of the reconstructable events satisfy the trigger criteria. Of the events passing the HLT cuts, about 65% come from the muon trigger chain, while the remaining 35% passed the electron trigger.

Table 6: Selection and HLT trigger acceptance and solution finding efficiency for signal and background.

$\tan\beta = 50$, $30\,\mathrm{fb}^{-1}$	# events before cuts	# events after selection cuts	# events after HLT cuts
$\mathrm{t\bar{t}}$ background	16 800 000	15 736 (0.09%)	13 471 (85.6%)
$\mathrm{t\bar{t}b}/\mathrm{t\bar{t}j}$ background	20 340 000	23 593 (0.12%)	20 208 (85.7%)
$\mathrm{tH}^{\pm}$ ($m_{\mathrm{A}} = 250\,\mathrm{GeV}/c^2$)	54 644	769 (1.41%)	655 (85.2%)
$\mathrm{tH}^{\pm}$ ($m_{\mathrm{A}} = 300\,\mathrm{GeV}/c^2$)	36 681	659 (1.80%)	560 (85.0%)
$\mathrm{tH}^{\pm}$ ($m_{\mathrm{A}} = 350\,\mathrm{GeV}/c^2$)	23 988	492 (2.05%)	419 (85.2%)
$\mathrm{tH}^{\pm}$ ($m_{\mathrm{A}} = 400\,\mathrm{GeV}/c^2$)	16 176	381 (2.35%)	328 (86.2%)
$\mathrm{tH}^{\pm}$ ($m_{\mathrm{A}} = 450\,\mathrm{GeV}/c^2$)	10 888	270 (2.48%)	230 (85.2%)
$\mathrm{tH}^{\pm}$ ($m_{\mathrm{A}} = 500\,\mathrm{GeV}/c^2$)	7 472	198 (2.65%)	170 (86.0%)

4 Analysis Strategy

4.1 Event reconstruction

Starting from the complex final state (3), it is possible to reconstruct the charged Higgs boson mass. The invariant mass of two non–b jets is calculated from the reconstructed objects from CMSJET, and it is required to be contained in a given mass window around the $\mathrm{W}^{\pm}$ mass,

$$|m_{\mathrm{qq'}} - m_{\mathrm{W}^{\pm}}| < 30\,\mathrm{GeV}/c^2. \tag{6}$$

For leptonic W decays, the longitudinal component of the missing energy is not measured, but the $\mathrm{W}^{\pm}$ mass constraint can be used to calculate the longitudinal momentum of the neutrino, giving rise to none or two real solutions. The reconstructed $\mathrm{W}^{\pm}$'s are combined with the b–tagged jets to reconstruct top quark candidates. The invariant mass is required to have a value in a given mass range around the top mass:

$$|m_{\mathrm{W}^{\pm}\mathrm{b}} - m_{\mathrm{t}}| < 50\,\mathrm{GeV}/c^2. \tag{7}$$

In general several solutions fulfilling (6) as well as (7) exist, due to the combination of the $\mathrm{W}^{\pm}$'s and the b jets and as a consequence of the additional combinatorics induced by extra jets. If no solution is found, the event is discarded. More detail is given in the next section on how an optimal solution is chosen.

Each reconstructed top quark is combined with the remaining b–tagged jet, giving rise to a charged Higgs boson candidate. The case in which the $\mathrm{W}^{\pm}$ from $\mathrm{H}^{\pm} \to \mathrm{tb} \to \mathrm{W}^{\pm}\mathrm{bb}$ decays hadronically is called the hadronic solution, and the case where the $\mathrm{W}^{\pm}$ decays leptonically is called the leptonic solution. As the Higgs boson mass is a priori not known, both combinations with the remaining b are possible solutions and have to be taken into account, which leads to a large extra irreducible background from wrong tb combinations.

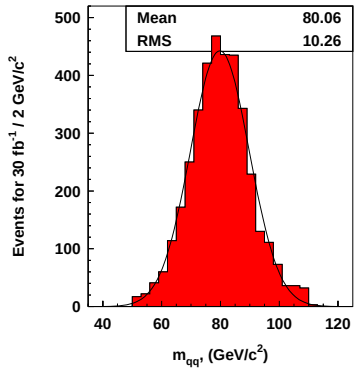

Figure 5: Reconstructed hadronic $\mathrm{W}^{\pm}$ mass with matched particles at generator level.

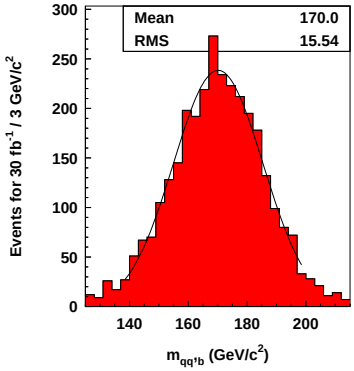

Figure 6: Reconstructed hadronic top mass with matched particles at generator level.

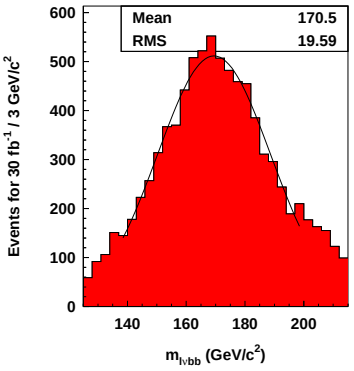

Figure 7: Reconstructed leptonic top mass with matched particles at generator level (except the neutrino).

The only further kinematical difference observed between the signal and background is the p_T spectrum of the b–tagged jet which is combined with the top quarks to form charged Higgs boson candidates. This spectrum is found to be harder in the signal samples than in the background samples, which gives a handle to further suppress the background. Therefore a cut on the transverse momentum of this reconstructed b was introduced,

$$p_T(\mathrm{b_{H^{\pm}}}) > 50\,\mathrm{GeV}/c. \tag{8}$$

4.2 Determination of the best solution

As there is no constraint on the Higgs boson mass, the only way to distinguish good from bad reconstructed solutions is by using the information from the $\mathrm{H}^{\pm}$ decay products. For this analysis, the following likelihood function is defined, starting from the reconstructed masses $m_{\mathrm{qq'b}}$ and $m_{\ell\nu\mathrm{b}}$ of both the reconstructed top quark candidates, and from the reconstructed mass $m_{\mathrm{qq'}}$ of the hadronic $\mathrm{W}^{\pm}$:

$$\begin{aligned}\mathcal{L} \;=\; & \exp\left[-\frac{1}{2}\left(\frac{m_{\mathrm{qq'}}-m^{*}_{\mathrm{qq'}}}{\sigma^{*}_{m_{\mathrm{qq'}}}}\right)^2\right]\times \\ & \exp\left[-\frac{1}{2}\left(\frac{m_{\mathrm{qq'b}}-m^{*}_{\mathrm{qq'b}}}{\sigma^{*}_{m_{\mathrm{qq'b}}}}\right)^2\right]\times\exp\left[-\frac{1}{2}\left(\frac{m_{\ell\nu\mathrm{b}}-m^{*}_{\ell\nu\mathrm{b}}}{\sigma^{*}_{m_{\ell\nu\mathrm{b}}}}\right)^2\right],\end{aligned} \tag{9}$$

The simulated distributions of the reconstructed mass values for the $\mathrm{W}^{\pm}$ and t candidates in all solutions, suffer from a large combinatorial background. Moreover, in the absence of jet energy calibration, the mean mass value in these distributions does not correspond to the real mass of the decayed particle.

To accommodate for these effects, the expected mean mass values $m^{*}_{\mathrm{qq'}}$, $m^{*}_{\mathrm{qq'b}}$ and $m^{*}_{\ell\nu\mathrm{b}}$ and resolutions $\sigma^{*}_{m_{\mathrm{qq'}}}$, $\sigma^{*}_{m_{\mathrm{qq'b}}}$ and $\sigma^{*}_{m_{\ell\nu\mathrm{b}}}$ should be estimated. In this analysis, the event generation information in the simulated samples is used. The distributions with the reconstructed masses are made, only for those solutions where the reconstructed jets and/or lepton are correctly matched to the particles at generator level they come from. This matching is performed by requiring that the reconstructed and generated particle are within a distance

$$\Delta R = \sqrt{\Delta\phi^2+\Delta\eta^2} < 0.2\,\mathrm{rad}. \tag{10}$$

In Figs. 5, 6 and 7, these mass distributions are shown for the t and $\mathrm{W}^{\pm}$ masses. For the $\mathrm{W}^{\pm}$ the distribution is centred around the real $\mathrm{W}^{\pm}$ mass, and has a good resolution. This distribution is similar to what can be obtained by correcting the jet energies according to [20]. When requiring a jet match with a generation level parton with a larger cone, radiated gluons worsen the resolution and move the mean mass value lower. The jet correction functions, proposed in [20], can unfortunately not directly be used in this study, as the parameters for the jet reconstruction algorithm differ. It leads to an overestimation of the energy of the jets when applying the corrections here. It is especially true for light jets, as the corrections are large in this case.

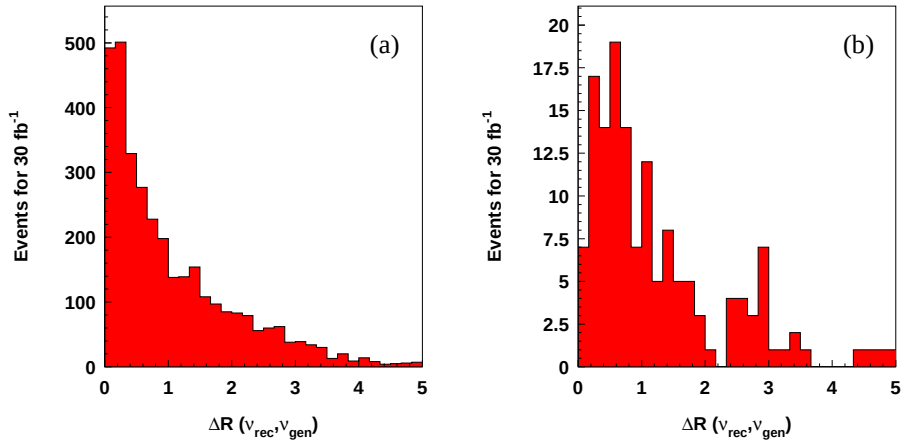

Figure 8: Distance $\Delta R = \sqrt{\Delta\eta^2 + \Delta\phi^2}$ between reconstructed and generated neutrino, for (a) background and (b) signal ($30\,\mathrm{fb}^{-1}$, $m_\mathrm{A} = 300\,\mathrm{GeV}/c^2$, $\tan\beta = 50$).

For the b jets, two effects play an important rôle: the gluon radiation of partons before hadronization, and the possible leptonic decay in b jets, giving rise to a missing energy from neutrinos. This second effect is indeed observed in the distributions for the top quarks with matching jets that have a lower mean mass value than the generated top mass, even if (10) is applied.

A final observation from the mass distributions is that a better resolution is achieved for the hadronically decaying top. It is expected because for the leptonically decaying top, the missing energy is used as transverse momentum for the neutrino, with no such constraint as (10). Other sources of missing energy in the event are not taken into account, and thus a poorer mass resolution is obtained. This effect is shown in Fig. 8, where the distribution of the distance ΔR between the reconstructed neutrino and the originating neutrino at generator level is displayed, for the events in the leptonic top mass distribution with b jet and lepton matching particles at generator level. A peak at $\Delta R = 0$ is observed, but there is also a long tail towards larger values.

For each event, the best solution is determined as that maximizing the likelihood function (9). The distribution of this value $\mathcal{L}$ for the best solution has a similar shape for background and signal. No cut is therefore applied on $\mathcal{L}$, in order not to further reduce the signal statistics.

4.3 Reconstruction efficiency

The final number of events, having at least one solution fulfilling (6), (7) and (8), as well as having a solution for the longitudinal momentum of the neutrino, is shown in Table 7.

Table 7: HLT trigger acceptance and solution finding efficiency for signal and background.

$\tan\beta = 50$, $30\,\mathrm{fb}^{-1}$	# events before cuts	# events after selection & HLT cuts	# events with $\geq$ one solution
$\mathrm{t\bar{t}}$ background	16 800 000	13 471 (0.08%)	4 932 (37%)
$\mathrm{t\bar{t}b}/\mathrm{t\bar{t}j}$ background	20 340 000	20 208 (0.10%)	7 872 (39%)
$\mathrm{tH}^\pm$ ($m_\mathrm{A} = 250\,\mathrm{GeV}/c^2$)	54 644	655 (1.22%)	314 (48%)
$\mathrm{tH}^\pm$ ($m_\mathrm{A} = 300\,\mathrm{GeV}/c^2$)	36 681	560 (1.53%)	235 (42%)
$\mathrm{tH}^\pm$ ($m_\mathrm{A} = 350\,\mathrm{GeV}/c^2$)	23 988	419 (1.75%)	173 (41%)
$\mathrm{tH}^\pm$ ($m_\mathrm{A} = 400\,\mathrm{GeV}/c^2$)	16 176	328 (2.03%)	116 (35%)
$\mathrm{tH}^\pm$ ($m_\mathrm{A} = 450\,\mathrm{GeV}/c^2$)	10 888	230 (2.11%)	86 (37%)
$\mathrm{tH}^\pm$ ($m_\mathrm{A} = 500\,\mathrm{GeV}/c^2$)	7 472	170 (2.28%)	72 (42%)

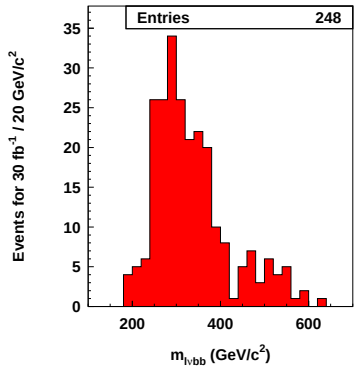

Figure 9: Leptonic solution of the charged Higgs boson mass for the signal ($m_{\mathrm{A}} = 300\,\mathrm{GeV}/c^2$, $\tan\beta = 50$).

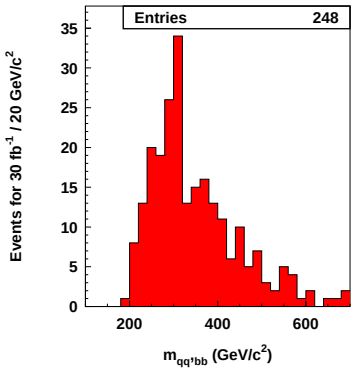

Figure 10: Hadronic solution of the charged Higgs boson mass for the signal ($m_{\mathrm{A}} = 300\,\mathrm{GeV}/c^2$, $\tan\beta = 50$).

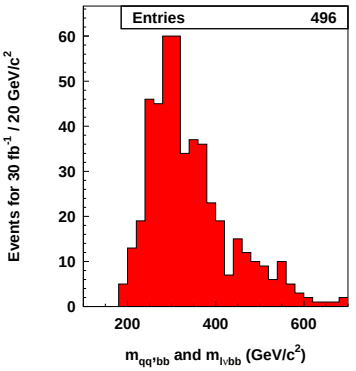

Figure 11: Sum of the leptonic and hadronic solutions of the charged Higgs boson mass for the signal ($m_{\mathrm{A}} = 300\,\mathrm{GeV}/c^2$, $\tan\beta = 50$).

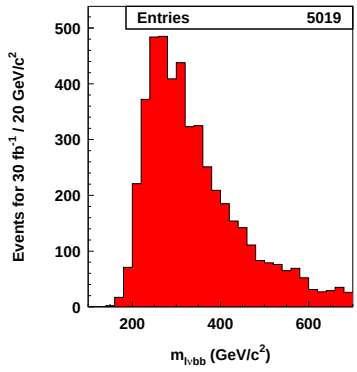

Figure 12: Leptonic solution of the charged Higgs boson mass for the background ($m_{\mathrm{A}} = 300\,\mathrm{GeV}/c^2$, $\tan\beta = 50$).

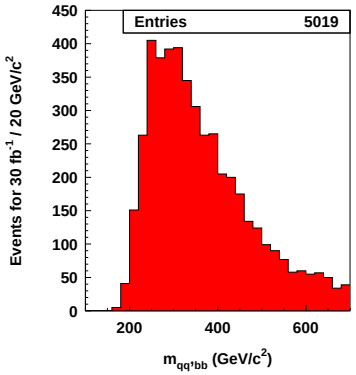

Figure 13: Hadronic solution of the charged Higgs boson mass for the background ($m_{\mathrm{A}} = 300\,\mathrm{GeV}/c^2$, $\tan\beta = 50$).

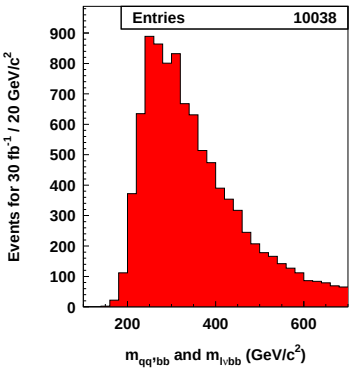

Figure 14: Sum of the leptonic and hadronic solutions of the charged Higgs boson mass for the background ($m_{\mathrm{A}} = 300\,\mathrm{GeV}/c^2$, $\tan\beta = 50$).

5 Results and Discussion

5.1 Mass distributions

In Figs. 9 and 10, the reconstructed invariant mass of the charged Higgs bosons is shown, respectively for the leptonic solution, built from the leptonically decaying top, and the hadronic solution, built from the hadronically decaying top, for the signal at $m_{\mathrm{A}} = 300\,\mathrm{GeV}/c^2$ and $\tan\beta = 50$ after $30\,\mathrm{fb}^{-1}$ integrated luminosity. Because of the ambiguity between both solutions, they have to be added up (Fig. 11). In Figs. 12, 13 and 14, the corresponding distributions are presented for the $\mathrm{t\bar{t}}$ background. For the $\mathrm{t\bar{t}b}/\mathrm{t\bar{t}j}$ background, these distributions are very similar as for $\mathrm{t\bar{t}}$, apart from an overall increase of the number of events. In Fig. 15, the total signal is shown on top of the $\mathrm{t\bar{t}}$ background.

The combinatorial background is large, which is mostly due to the irreducible background from the two Higgs boson mass solutions, of which one is always wrong. Another contribution is attributed to the relatively poor reconstruction efficiency for the neutrino, as previously illustrated by the distribution of Fig. 8.

In Fig. 16 finally, the sum of leptonic and hadronic solutions of the Higgs boson mass is shown, for the signal, background and the sum of both, for $m_{\mathrm{A}} = 400\,\mathrm{GeV}/c^2$ and $\tan\beta = 50$.

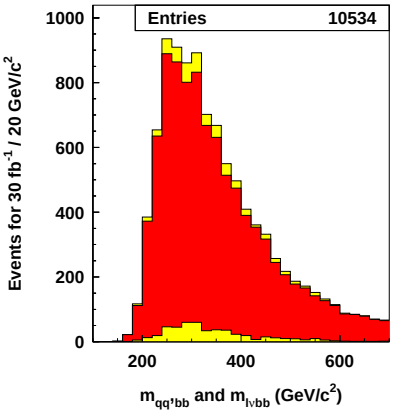

Figure 15: Sum of the leptonic and hadronic solutions of the charged Higgs boson mass for the signal, the background and the sum of the background and the signal ($m_{\mathrm{A}} = 300\,\mathrm{GeV}/c^2$, $\tan\beta = 50$).

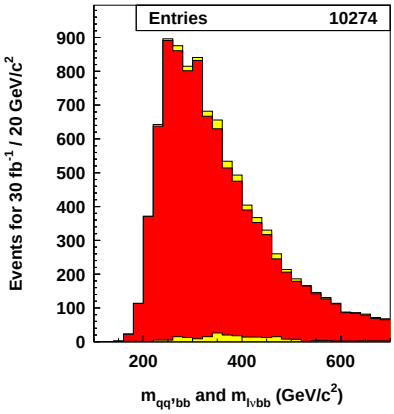

Figure 16: Sum of the leptonic and hadronic solutions of the charged Higgs boson mass for the signal, the background and the sum of the background and the signal ($m_{\mathrm{A}} = 400\,\mathrm{GeV}/c^2$, $\tan\beta = 50$).

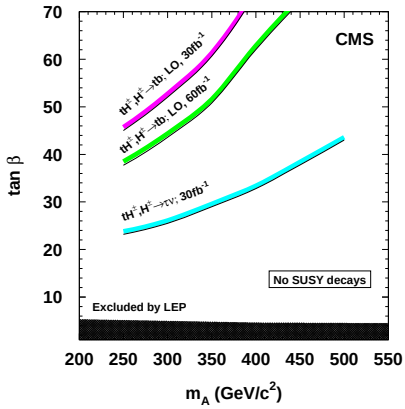

Figure 17: Discovery contours for the $\mathrm{tH}^{\pm}, \mathrm{H}^{\pm} \to \mathrm{tb}$ channel with $30\,\mathrm{fb}^{-1}$ and $60\,\mathrm{fb}^{-1}$, and for the $\mathrm{tH}^{\pm}, \mathrm{H}^{\pm} \to \tau\nu$ channel with $30\,\mathrm{fb}^{-1}$.

5.2 Signal significance and discovery contours

In this section the significance at low luminosity in the CMS experiment is estimated. No systematic uncertainties are included at this point, to be able to make comparisons with previous results. The discovery potential, however, is strongly affected by systematic uncertainties, as discussed in Section 5.3.

Because of the presence of the large number of background events, the statistical significance of the signal is calculated as $\sigma = S/\sqrt{B}$, where S and B denote the number of signal and background events respectively. All entries in the histograms were counted. If instead a mass window around the charged Higgs boson mass is taken to calculate the significance, the results for the region of interest of lower masses get worse, because of the too strongly reduced signal statistics compared to the background. The signal–to–noise ratio however improves. By including jet calibration, especially for b jets, and rescaling the jet energies to fit the $\mathrm{W}^{\pm}$ and t masses after reconstruction, the resolution on the correctly reconstructed Higgs boson masses can still be further improved. The significance calculated in a smaller mass window might then improve, but it has not been considered yet in this analysis.

The 5σ–discovery contour for an integrated luminosity of $30\,\mathrm{fb}^{-1}$ and $60\,\mathrm{fb}^{-1}$ is shown in Fig. 17, with the $\mathrm{t\bar{t}}$ background. In the same plot, also the current discovery contour is shown for the subdominant decay channel, $\mathrm{H}^{\pm} \to \tau\nu$, for $30\,\mathrm{fb}^{-1}$ of integrated luminosity [21].

When comparing the discovery contour for $\mathrm{H}^{\pm} \to \mathrm{tb}$ to the previous similar studies in CMS [7] and ATLAS [8,9], a similar shape is observed, but also a very large difference in position of the contour in the $(m_{\mathrm{A}}, \tan\beta)$ plane. This

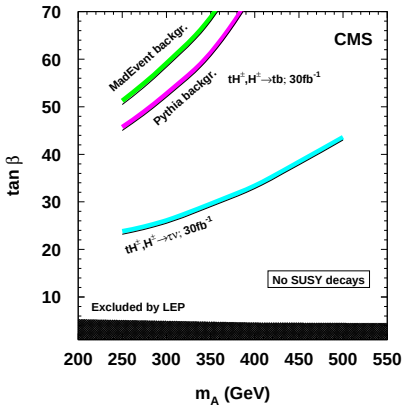

Figure 18: Discovery contours for the $\mathrm{tH}^{\pm}, \mathrm{H}^{\pm} \rightarrow \mathrm{tb}$ channel with $30\,\mathrm{fb}^{-1}$, for the backgrounds $\mathrm{t\bar{t}}$ from `PYTHIA`, and $\mathrm{t\bar{t}b}/\mathrm{t\bar{t}j}$ from `MadGraph/MadEvent`.

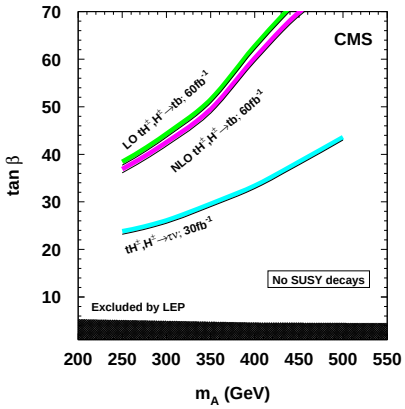

Figure 19: Discovery contours at LO and NLO for $60\,\mathrm{fb}^{-1}$, using k factors for signal and $\mathrm{t\bar{t}}$ background.

difference was investigated with respect to the previous CMS result, and found to be due to the large drop in the signal cross section, described in Section 2.1. This analysis was repeated with the cuts used in the previous study, selecting events in the $\mathrm{t\bar{t}}$ background sample simulated for this study. The selection efficiencies agreed within 2% with the previous results on a similarly generated background sample.

The influence of the chosen background sample on the discovery potential, was also investigated. The $\mathrm{t\bar{t}b}/\mathrm{t\bar{t}j}$ background was found to have a larger cross section on the one hand, and larger selection efficiencies on the other, mainly due to a larger b–mistag rate. This increase of the background is reflected in the position of the discovery contours. In Fig. 18 both contours are drawn for an integrated luminosity of $30\,\mathrm{fb}^{-1}$.

As was stated before, no next–to–leading order calculation has yet been performed for the $\mathrm{t\bar{t}b}/\mathrm{t\bar{t}j}$ background. For the $\mathrm{t\bar{t}}$ background, results at LO and NLO can be compared using k factors. The effect of such a scaling of signal and background is shown in Fig. 19.

5.3 Influence of systematic uncertainties on the background cross section

For small values of m_{A}, the signal Higgs boson mass peak coincides with the peak from the background. For larger masses the signal peak becomes wider, and the number of signal events decreases. In addition, the combinatorial background always has the same distribution as the real background. For these reasons, the analysis is in practice limited to be a counting experiment.

So far in this study, the significance was calculated in the ideal case of perfect knowledge of the background cross section. The background is large, however, and with the previous considerations in mind, the effect of systematic uncertainties on the knowledge of the background should be estimated. In order to measure the background cross section level and uncertainty from the data, a signal free sample should be obtained. For this analysis, however, the signal and background are kinematically very similar, and the combinatorial background is omnipresent in the studied distributions.

5.3.1 Estimation of the background rate from data

The spectrum of the b–tagged jet, combined with the top quarks to form charged Higgs boson candidates, was found to be harder in the signal samples than in the background samples. An upper bound on this spectrum allows for the selection of an event sample with suppressed signal contribution. When taking this cut too low the statistical uncertainty on the obtained background level is large. For $p_T < 30\,\mathrm{GeV}/c$ for example, 400 background events remain, leading to a statistical uncertainty of 5%. With a less stringent cut on the other hand, the remaining signal in the sample also becomes a few percent at small m_{A}. Both sources of uncertainty together, minimally yield a 5% uncertainty on the measured background level. Moreover, this procedure of cutting on the transverse momentum of the b–tagged jet, assumed to come from the Higgs boson decay, is sensitive to theoretical uncertainties, related to the shape of the p_T distributions of all the jets in the event, especially the b jet from the Higgs boson decay. This theoretical contribution can additionally lead to sizeable systematic uncertainties.

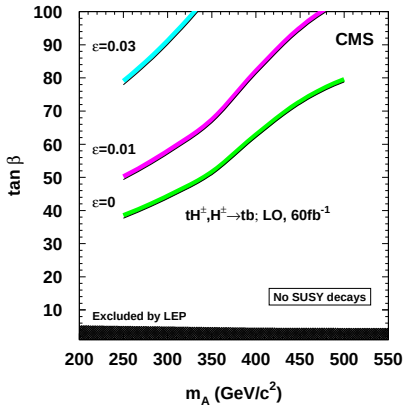

Figure 20: Discovery contours with systematic uncertainties ϵ (0%, 1% and 3%) on the total background cross section, for $60\,\mathrm{fb}^{-1}$.

Another way to estimate the background level from data, is to impose the same, or harder, selection cuts on the data as in Section 3, but to require one b–tagged jet less. It has been shown that, even with two b–tagged jets, the main background remains $\mathrm{t\bar{t}} + \mathrm{jets}$ [14]. After such a selection with only two b–tagged jets, the signal is much smaller than the background. It is then possible to calculate the expected number of background events plus its uncertainty, when tagging a third b jet. For this method, a measured b–tagging efficiency and purity is needed from data. In such a calculation for the background, the main uncertainty comes from the uncertainty on the b–tagging purity. Supposing an uncertainty on the mistag probability of 10%, as for instance found as systematic uncertainty in CDF for the b–tagging mistag probability obtained by the secondary vertex tag technique [19], then the uncertainty on the background rate is of the order of 7%, when selecting 10 000 events with only two b–tagged jets. Possibly large theoretical uncertainties should also be taken into account, like the ratio of events with real extra b jets and events with only light jets accompanying the top quarks.

5.3.2 Estimation of the background rate from theoretical calculations

In the absence of an experimental method to measure the background, its uncertainty can be estimated using the theoretically calculated cross section, the luminosity and the reconstruction and analysis efficiencies. When estimating the background uncertainty this way, a typical contribution of about 10 to 15% systematic uncertainty is expected from the not yet available calculation of the NLO background cross section. With an additional optimistic 5% systematic uncertainty for the contribution from the CMS/TOTEM measurement of the luminosity, the total uncertainty on the background rate is estimated to be at least 15%. Additionally, systematic uncertainties on the analysis and reconstruction efficiencies may be sizeable.

5.3.3 Influence of background systematic uncertainties on the signal visibility

With these systematic uncertainty estimates from different methods, the effects on the visibility of the signal can be evaluated. Considering a systematic uncertainty ϵ on the total cross section, an uncertainty of ϵB events on the number of background events B after the full analysis, has to be accounted for. Adding this uncertainty to the statistical one in quadrature, a total uncertainty $\Delta B = \sqrt{(\sqrt{B})^2 + (\epsilon B)^2} = \sqrt{B + \epsilon^2 B^2}$ on the number of background events is obtained. The signal significance for S signal events now becomes $\sigma = S/\sqrt{B + \epsilon^2 B^2}$.

It is clear that the value of S/B has to be sufficiently large, for this systematic contribution $\epsilon^2 B^2$ to be kept under control. In this channel, the background is too large, which does not allow S/B to be improved sufficiently without losing too much signal statistics. In Fig. 20 the discovery contours are plotted, when supposing perfect knowledge of the $\mathrm{t\bar{t}}$ cross section ($\epsilon = 0$), a 1% uncertainty ($\epsilon = 0.01$), and a 3% uncertainty ($\epsilon = 0.03$). A value of 5% already is no longer visible in the figure. From the above estimates of the systematic uncertainty on the number of background events, the conclusion is drawn that no visibility for this channel with triple b tagging is left in the MSSM parameter space at low luminosity.

6 Fully hadronic channel

A further possibility to extend the reach of the current channel is to include other decay modes. As for the fully leptonic channel two neutrinos are present that blur the kinematics, an attempt was done to use the fully hadronic decay channel. Because of the absence of neutrinos in the final state, the resolution of the reconstructed Higgs boson mass is expected to be better than in the semileptonic decay channel.

For the fully hadronic channel, there is no lepton to trigger on and because of this absence of a lepton, the acceptance of the CMS triggers was considered in detail first. The Level–1 hardware trigger as well as the High Level software Trigger were studied. The cuts are taken again as in [18] for the low luminosity phase of the LHC. The one, three or four jets trigger chains were considered. In Table 8 the results of these trigger cuts on the different samples are shown for $30\,\mathrm{fb}^{-1}$ and $\tan\beta = 30$. The event rates after Level–1 are still acceptable, but the HLT cuts remove almost all events. In addition the selection and analysis efficiencies have to be taken into account. Moreover, the $\mathrm{t\bar{t}}$ background is again very large, and other multi–jet sources may contribute as well to the total background. As a conclusion, without an HLT b trigger, no hope is left for this decay channel.

Table 8: Level–1 and HLT trigger acceptance for signal and background in the fully hadronic decay channel. The numbers quoted are at $\tan\beta = 30$ and for $30\,\mathrm{fb}^{-1}$ integrated luminosity.

$\tan\beta = 30$	# events at $30\,\mathrm{fb}^{-1}$	# events after Level–1 cuts	# events after HLT cuts
$\mathrm{t\bar{t}}$ background	16 800 000	3 389 559 (20.2%)	141 789 (0.84%)
$\mathrm{tH}^{\pm}$ ($m_{\mathrm{A}} = 250\,\mathrm{GeV}/c^2$)	19 707	5 133 (26.0%)	251 (1.28%)
$\mathrm{tH}^{\pm}$ ($m_{\mathrm{A}} = 300\,\mathrm{GeV}/c^2$)	13 227	4 661 (35.2%)	253 (1.92%)
$\mathrm{tH}^{\pm}$ ($m_{\mathrm{A}} = 350\,\mathrm{GeV}/c^2$)	8 649	3 950 (45.7%)	255 (2.95%)
$\mathrm{tH}^{\pm}$ ($m_{\mathrm{A}} = 400\,\mathrm{GeV}/c^2$)	5 833	3 337 (57.2%)	258 (4.42%)
$\mathrm{tH}^{\pm}$ ($m_{\mathrm{A}} = 450\,\mathrm{GeV}/c^2$)	3 926	2 603 (66.3%)	224 (5.71%)
$\mathrm{tH}^{\pm}$ ($m_{\mathrm{A}} = 500\,\mathrm{GeV}/c^2$)	2 694	2 007 (74.5%)	201 (7.45%)

7 Conclusion

In this paper the prospects to discover a heavy charged MSSM Higgs boson in the $\mathrm{H}^{\pm} \rightarrow \mathrm{tb}$ decay in CMS during the low luminosity run of the LHC have been presented. The charged Higgs boson has been produced in the $\mathrm{pp} \rightarrow \mathrm{tH}^{\pm}\mathrm{X}$ channel. Cascades from heavy sparticles and decays into lighter SUSY particles have not not considered. The only important background for this channel, $\mathrm{t\bar{t}} + \mathrm{jets}$, is large and kinematically very similar to the signal.

The detailed event selection and reconstruction, performed with the fast CMS detector simulation, including the HLT acceptance, was described. Tagging of b jets was found to be the most important tool to suppress the background. Three b–tagged jets were required in this analysis. Emphasis was further put on the problems of the combinatorial background, which appears in different forms. A scheme was presented to choose the best solution, according to the value of a likelihood function, built from distributions where the reconstructed jets and/or lepton match the particles at generator level. The charged Higgs boson mass was reconstructed and the 5σ–discovery contour in the $(m_{\mathrm{A}}, \tan\beta)$ plane was presented.

Several improvements were made with respect to previous results [7]. The most recent cross section values were used, differing much from previous predictions. A dedicated background simulation of the $\mathrm{t\bar{t}b}/\mathrm{t\bar{t}j}$ background was performed, showing a significant increase in the background compared to the $\mathrm{t\bar{t}}$ background. The influence of a systematic uncertainty on the total background cross section was evaluated, and found to have a large effect on the visibility of the signal, due to the very small signal–to–noise ratio.

As a conclusion for this decay channel with triple b tagging, no visibility is left in the MSSM parameter space, due to the large effects of systematic uncertainties on the background.

Acknowledgments

We would like to thank F. Maltoni, A. Nikitenko, T. Plehn and D. Rainwater for the helpful discussions. Also many thanks to the people in the Brussels CMS group for their help and support.

References

[1] J. F. Gunion, H. E. Haber, G. L. Kane, and S. Dawson, *The Higgs Hunters' Guide*. Addison-Wesley, Reading, MA, 1990.

[2] V. D. Barger, R. J. N. Phillips, and D. P. Roy, Phys. Lett. **B324** (1994) 236–240.

[3] J. F. Gunion, Phys. Lett. **B322** (1994) 125–130.

[4] S. Moretti and D. P. Roy, Phys. Lett. **B470** (1999) 209–214.

[5] D. J. Miller, S. Moretti, D. P. Roy, and W. J. Stirling, Phys. Rev. **D61** (2000) 055011.

[6] D. Cavalli *et al.*, *The Higgs working group: Summary report*, `hep-ph/0203056`.

[7] P. Salmi, R. Kinnunen, and N. Stepanov, *Prospects of Detecting Massive Charged Higgs from Hadronic Decay $H^{\pm} \to tb$ in CMS*, CMS NOTE 2002/024, 2002.

[8] K. A. Assamagan, *The Charged Higgs in Hadronic Decays with the ATLAS Detector*, ATLAS-PHYS-99-017, 1999.

[9] K. A. Assamagan and Y. Coadou, *Prospects for the Determination of the Charged Higgs Mass and $\tan\beta$ with ATLAS*, ATLAS-PHYS-2001-017, 2001.

[10] T. Plehn, Phys. Rev. **D67** (2003) 014–018.

[11] T. Sjostrand *et al.*, Comput. Phys. Commun. **135** (2001) 238–259.

[12] A. Djouadi, J. Kalinowski, and M. Spira, Comput. Phys. Commun. **108** (1998) 56–74.

[13] T. Plehn, Private communication.

[14] L. Sonnenschein, *Top mass determination in the $t\bar{t}$ semileptonic decay channel*, CMS NOTE 2001/001, 2001.

[15] F. Maltoni and T. Stelzer, JHEP **02** (2003) 027.

[16] G. Altarelli and M.L. Mangano (eds.), *Standard Model Physics (and more) at the LHC. Proceedings, Workshop, Geneva, Switzerland, May 25-26, October 14-15, 1999*, Geneva, Switzerland, CERN (2000).

[17] S. Abdullin, *CMSJET*, CMS TN/94-180 (version of 10/10/2001), 2001.

[18] CMS Collaboration, *Technical Design Report: The TriDAS Project, Volume II: Data Acquisition & High Level Trigger*, CERN/LHCC/2002-26, 2002.

[19] CDF Collaboration, T. Affolder *et al.*, Phys. Rev. **D64** (2001) 032002.

[20] V. Drollinger, *Jet Energy Corrections*, CMS NOTE 1999/066, 1999.

[21] R. Kinnunen, *Study for Heavy Charged Higgs in $pp \to tH^{\pm}$ with $H^{\pm} \to \tau\nu$ in CMS*, CMS NOTE 2000/045, 2000.